CM² MAGAZINE

第 103 期

南方科技大学海洋磁学中心主编

http://cm2.sustech.edu.cn/

创刊词

海洋是生命的摇篮，是文明的纽带。地球上最早的生命诞生于海洋，海洋里的生命最终进化成了人类，人类的文化融合又通过海洋得以实现。人因海而兴。

人类对海洋的探索从未停止。从远古时代美丽的神话传说，到麦哲伦的全球航行，再到现代对大洋的科学钻探计划，海洋逐渐从人类敬畏崇拜幻想的精神寄托演变成可以开发利用与科学研究的客观存在。其中，上个世纪与太空探索同步发展的大洋科学钻探计划将人类对海洋的认知推向了崭新的纬度：深海（deep sea）与深时（deep time）。大洋钻探计划让人类知道，奔流不息的大海之下，埋藏的却是亿万年的地球历史。它们记录了地球板块的运动，从而使板块构造学说得到证实；它们记录了地球环境的演变，从而让古海洋学方兴未艾。

在探索海洋的悠久历史中，从大航海时代的导航，到大洋钻探计划中不可或缺的磁性地层学，磁学发挥了不可替代的作用。这不是偶然，因为从微观到宏观，磁性是最基本的物理属性之一，可以说，万物皆有磁性。基于课题组的学科背景和对海洋的理解，我们对海洋的探索以磁学为主要手段，海洋磁学中心因此而生。

海洋磁学中心，简称 CM^2，一为其全名“Centre for Marine Magnetism”的缩写，另者恰与爱因斯坦著名的质能方程 $E = MC^2$ 对称，借以表达我们对科学巨匠的敬仰和对科学的不懈追求。

然而科学从来不是单打独斗的产物。我们以磁学为研究海洋的主攻利器，但绝不仅限于磁学。凡与磁学相关的领域均是我们关注的重点。为了跟踪反映国内外地球科学特别是与磁学有关的地球科学领域的最新研究进展，海洋磁学中心特地主办 CM^2 Magazine，以期与各位地球科学工作者相互交流学习、合作共进！

“海洋孕育了生命，联通了世界，促进了发展”。21 世纪是海洋科学的时代，由陆向海，让我们携手迈进中国海洋科学的黄金时代。

目录

1. 对 2.5 亿年“氧通气”记录间隔的重新检验表明在大氧化事件之前海洋就是缺氧的

翻译人：王敦繁 Dunfan-w@foxmail.com

Sarah P. Slotznick, Jena E. Johnson, Birger Rasmussen, Timothy D. Raub, Samuel M. Webb, Jian-Wei Zi, Joseph L. Kirschvink, Woodward W. Fischer. ***Reexamination of 2.5-Ga “whiff” of oxygen interval points to anoxic ocean before GOE [J].*** *Science Advances, 2022, 8, eabj7190.*

https://doi. org/10.1126/sciadv.abj7190

摘要：根据对氧化还原反应敏感的元素(如 Mo 和 S)，在大氧化事件(GOE)之前[~ 23 亿年前(Ga)]，氧的短暂出现已经被推断出来，最主要的是来自西澳大利亚州的 McRae 山页岩~ 2.5 亿年。我们提供了新的空间解析数据，包括基于同步辐射的 x 射线光谱和二次离子质谱，以表征 McRae 页岩的岩石成因。沉积物主要由有机质和火山灰(Mo 的潜在来源)组成，U-Pb 年龄表明沉积速率极低。后成岩作用形成了层状平行微裂缝，进而成为交代蚀变和近期氧化风化作用的流体通道。我们的整合记录表明，大量的化学数据集指向沉积后事件中形成的“一股”氧气。在微量金属贫乏的早期成岩黄铁矿和异常富集的低沉积速率的有机碳中，$\Delta^{33}S$ 的非零值表明，在 GOE 之前的 1 亿 5 千万年前，环境中的氧水平可以忽略不计。

ABSTRACT: Transient appearances of oxygen have been inferred before the Great Oxygenation Event (GOE) [~2.3 billion years (Ga) ago] based on redox-sensitive elements such as Mo and S—most prominently from the ~2.5-Ga Mount McRae Shale in Western Australia. We present new spatially resolved data including synchrotron-based x-ray spectroscopy and secondary ion mass spectrometry to characterize the petrogenesis of the Mount McRae Shale. Sediments were primarily composed of organic matter and volcanic ash (a potential source of Mo), with U-Pb ages revealing extremely low sedimentation rates. Catagenesis created bedding-parallel microfractures, which subsequently acted as fluid pathways for metasomatic alteration and recent oxidative weathering. Our collective observations suggest that the bulk chemical datasets pointing toward a “whiff” of oxygen developed during postdepositional events. Nonzero $\Delta^{33}S$ in trace-metal–poor, early diagenetic pyrite and the unusually enriched organic carbon at low sedimentation rates instead suggest that environmental oxygen levels were negligible ~150 million years before the GOE.

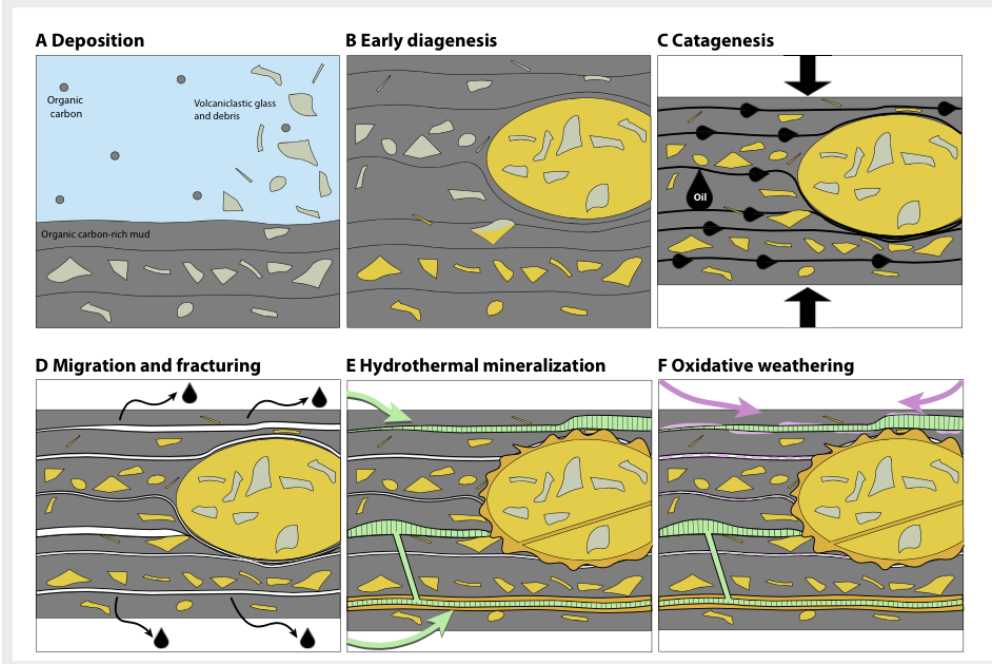

Figure 1. Schematic diagram of petrogenesis of Mount McRae Shale based on our observations and geochemical data. (A) Deposition of organic carbon and air-fall volcaniclastic debris. (B) Early stages of diagenesis including pyrite nodule growth and pyrite permineralization of sediments. (C) Compaction during burial and thermal maturation of organic-rich sediments in catagenesis. (D) Hydrocarbon formation leads to episodic fluid overpressure, microfracturing, and hydrocarbon expulsion along bedding-parallel microfractures eventually developing into fissile cleavage. (E) Migration of cratonic fluids along microfractures accompanied by at least three episodes of metasomatic mineralization, including pyrite rich in both As and Mo. (F) Introduction of meteoric fluids and oxidative weathering resulting in pyrite oxidation and calcium sulfate precipitation along fissile cleavage.

2. 在末次冰期东南大西洋地区持续性深水缺氧

翻译人：仲义 zhongy@sustech.edu.cn

Natascha Riedinger, Florian Scholz, Micchelle L. Abshire, and Matthias Zabel, ***Persistent deep water anoxia in the eastern South Atlantic during the last ice age*** *[J] PNAS, 2021, 118(49), e2107034118.*

https://www.pnas.org/content/pnas/118/49/e2107034118.full.pdf

摘要：在过去冰期阶段，海洋沉积物记录在水深大约>1500m 以下的海洋内部洋流通风作用不断减弱。不同海洋盆地中相关的氧含量消耗程度仍然未知。本文作者利用非洲大陆西南边缘地区的氧化还原性指标，记录显示在最后一次冰期期间，东南大西洋东部的底部水体持续性缺氧，会导致长时间碳埋藏的不断增强。地球化学数据表明，在上一个冰期内，南大西洋东部与上升流相关的生产力及其最低含氧带向远海移动，并在冰消期时慢慢后退。虽然末次冰期生产力不断升高可能会增加底层水的氧气消耗，从而减缓了晚第四纪以来的深水环流模式，并成为导致深水缺氧的最终原因。

ABSTRACT: During the last glacial interval, marine sediments recorded reduced current ventilation within the ocean interior below water depths of approximately >1,500 m [B. A. Hoogakker et al., Nat. Geosci. 8, 40–43 (2015)]. The degree of the associated oxygen depletion in the different ocean basins, however, is still poorly constrained. Here, we present sedimentary records of redox-sensitive metals from the southwest African margin. These records show evidence of continuous bottom water anoxia in the eastern South Atlantic during the last glaciation that led to enhanced carbon burial over a prolonged period of time. Our geochemical data indicate that upwelling-related productivity and the associated oxygen minimum zone in the eastern South Atlantic shifted far seaward during the last glacial period and only slowly retreated during deglaciation times. While increased productivity during the last ice age may have contributed to oxygen depletion in bottom waters, especially on the upper slope, slow-down of the Late Quaternary deep water circulation pattern [Rutberg et al., Nature 405, 935–938 (2000)] appears to be the ultimate driver of anoxic conditions in deep waters.

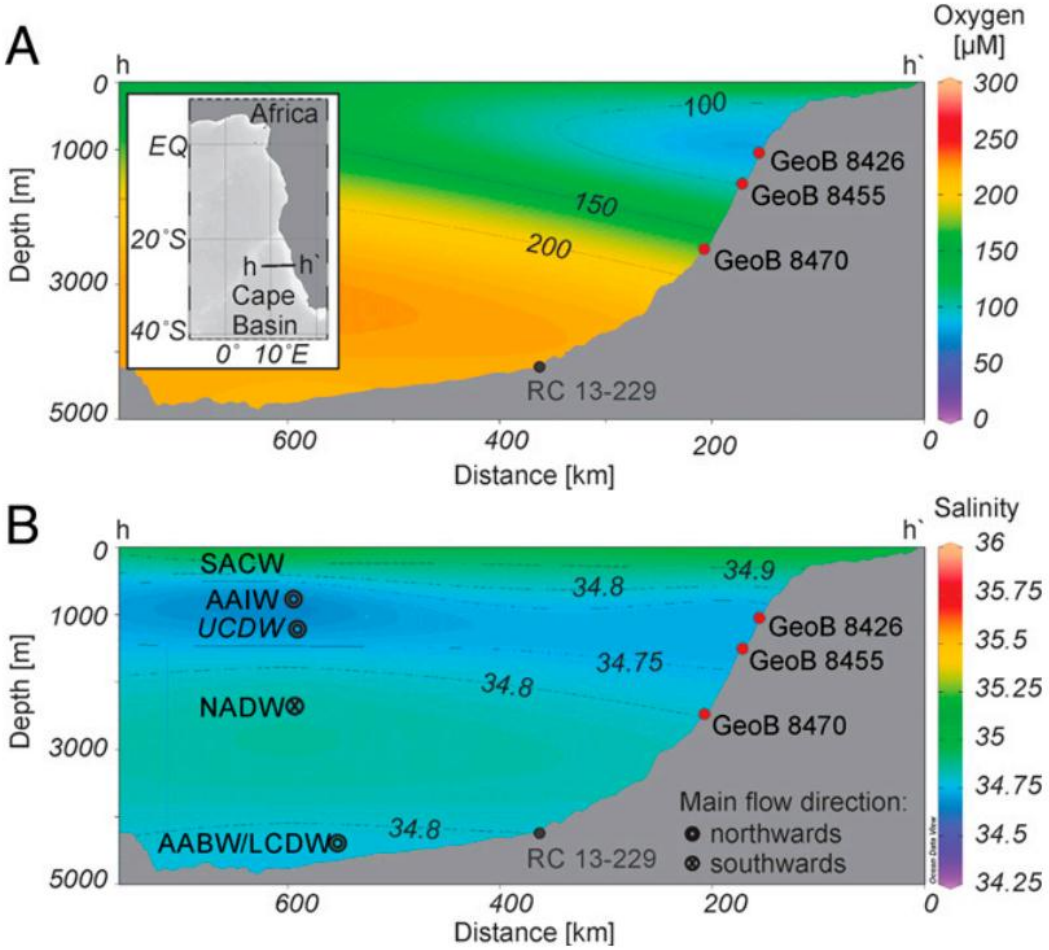

Figure 1. Modern oceanographic conditions along the study sites at the Namibian continental margin. (A) Cross-section of dissolved oxygen concentrations (O_2) displaying the present-day location of the OMZ and overview map. (B) Water column salinity with major currents and flow directions. The tropical surface waters are underlain by the South Atlantic Central Water (SACW). Originating from the Indian Ocean, the Antarctic Intermediate Water (AAIW) propagates northwards, similar to the Upper Circumpolar Deep Water (UCDW) which lies below the AAIW and originates from the Antarctic Circumpolar Current. Advecting southwards, the NADW is underlain by the northward propagating Lower Circumpolar Deep Water (LCDW) and Antarctic Bottom Water (AABW) (refer to ref. 6 and references therein). Plots were created using the software Ocean Data View (7). Red dots indicate study sites; dark gray dot shows the location of Site RC 13–229 (8).

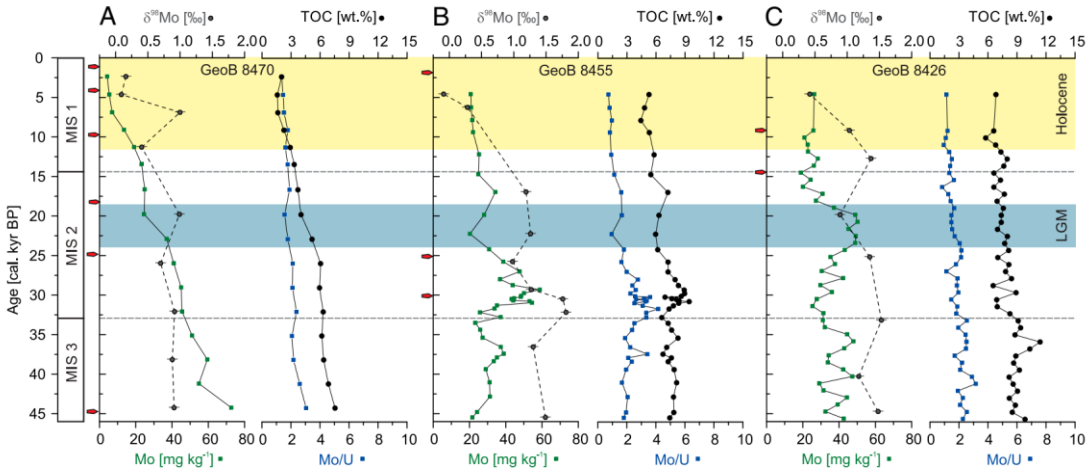

Figure 2. Reconstruction of the redox conditions for the last 46 ky along the Namibian Continental Margin. (A) TOC, molybdenum concentration (Mo), Mo isotope (δ^{98}Mo; 2SD), and Mo/U ratios for the lower slope Site GeoB 8470. (B and C) Geochemical data for the sites located on the upper slope, Sites GeoB 8455 and GeoB 8426, respectively. Red arrows depict 14C ages. The yellow bar indicates the Holocene (11.5 ky BP to present) and the gray bar the LGM (24 to 18.7 ky BP) interval within the respective MIS.

3. 过去千年中亚洲-澳大利亚季风演化与石笋 $\delta^{18}O$ 中记录的联系

翻译人：王浩森 11930841@mail.sustech.edu.cn

Zhang, J., Liang, M.-Q., Li, T.-Y., Chen, C.-J., Li, J.-Y., ***Asian-Australian monsoon evolution over the last millennium linked to ENSO in composite stalagmite $\delta^{18}O$ records.*** *Quaternary Science Reviews 2022. 281, 107420.*

https://doi.org/10.1016/j.quascirev.2022.107420

摘要：亚洲-澳大利亚季风（AAM）系统会明显影响全球气候。然而，在过去的千年里，人们对 ENSO（厄尔尼诺-南方涛动）与 AAM 之间的联系仍然了解较少。本文将石笋 $\delta^{18}O$（$\delta^{18}O_s$）记录与高分辨率和高精度年表相结合，以证明 AAM 与热带海洋水文在多年、十年和百年时间尺度上的紧密遥相关。我们的结果表明：（1）AAM 的多年加权平均降水量 $\delta^{18}O$（$\delta^{18}O_{aw}$）与南方涛动指数（SOI）之间存在显著的负相关，为过去 100 年来石笋 $\delta^{18}O$（$\delta^{18}O_s$）与 ENSO 之间的联系提供了一个现代类似的相关。（2）在过去的千年中，$\delta^{18}O_s$ 的记录在小冰河时期（LIA）出现正偏移，其特征是热带太平洋出现更多类似厄尔尼诺的状态，这与 SST 梯度重建的 ENSO 是一致的，但与降水重建不同。（3）对 AAM 地区 $\delta^{18}O_s$ 综合记录的小波和能谱分析表明，与 ENSO 循环（2-7 年）相比，存在显著的多年周期性（2.2、2.8、3.5、4.6 年），而一些数十年和百年周期（10.1、17、28.6、52.7、143 年）也具有显著性。我们提供了来自仪器和古气候数据（GNIP 和 NOAA）的证据，并提出了一种可能的“环流效应”机制，该机制能够解释东亚季风（EAM）和澳大利亚季风（AM）地区过去千年 $\delta^{18}O_s$ 的变化。

ABSTRACT: The Asian-Australian monsoon (AAM) system distinctly influences global climate. However, the linkage between ENSO (El Niño–Southern Oscillation) and AAM is still poorly understood over the last millennium. Here, we combined stalagmite $\delta^{18}O$ ($\delta^{18}O_s$) records with exceptionally high-resolution and high-precision chronologies to demonstrate a tight remote coupling between AAM and tropical ocean hydrology on the multi-year, decadal, and centennial timescales. Our results reveal that (1) There is a significant negative correlation between the multi-year weighted average precipitation $\delta^{18}O$ ($\delta^{18}O_{aw}$) from the AAM and Southern Oscillation Index (SOI), providing a modern analogous coupling for linking stalagmite $\delta^{18}O$ ($\delta^{18}O_s$) and ENSO over

the past 100 years. (2) Over the last millennium, the integrated $\delta^{18}O_s$ record exhibit positive excursions during the Little Ice Age (LIA), marked by a tendency for more El Niño-like state conditions in the tropical Pacific, which is consistent in SST-gradient ENSO reconstruction but different to precipitation reconstruction. (3) Wavelet and power spectrum analysis for the integrated $\delta^{18}O_s$ record in the AAM region show that there is a significant multi-year periodicity (2.2, 2.8, 3.5, 4.6 yr), conceding with the ENSO cycle (2–7 yr), whereas, some multi-decadal and centennial cycles (10.1, 17, 28.6, 52.7, 143 yr) are significant too. We provide evidence from instrumental and paleocliamte datasets (GNIP and NOAA) and propose a possible "circulation effect" mechanism responsible for variations of δ18Os in the East Asian Monsoon (EAM) and Australian Monsoon (AM) region over the last millennium.

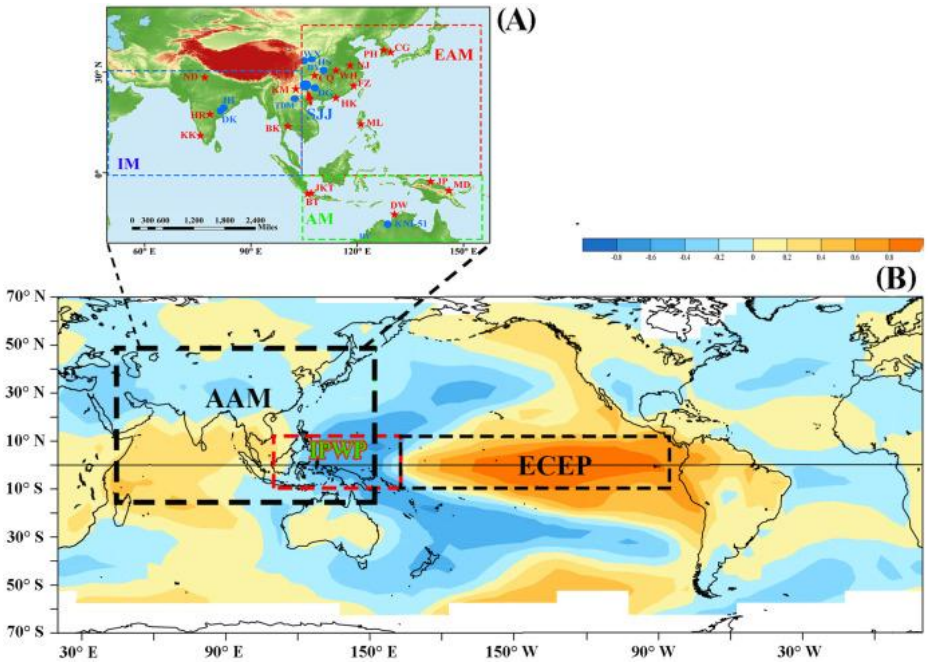

Figure 1. (A) Distribution of GNIP meteorological stations (red stars) and stalagmite records (blue dots) in this study. (B) Typical El Niño years' sea-surface temperature (SST) anomalies in Niño 3.4 zone correlated with global surface temperature for all calendar months during the period 1979–2006 (CE).

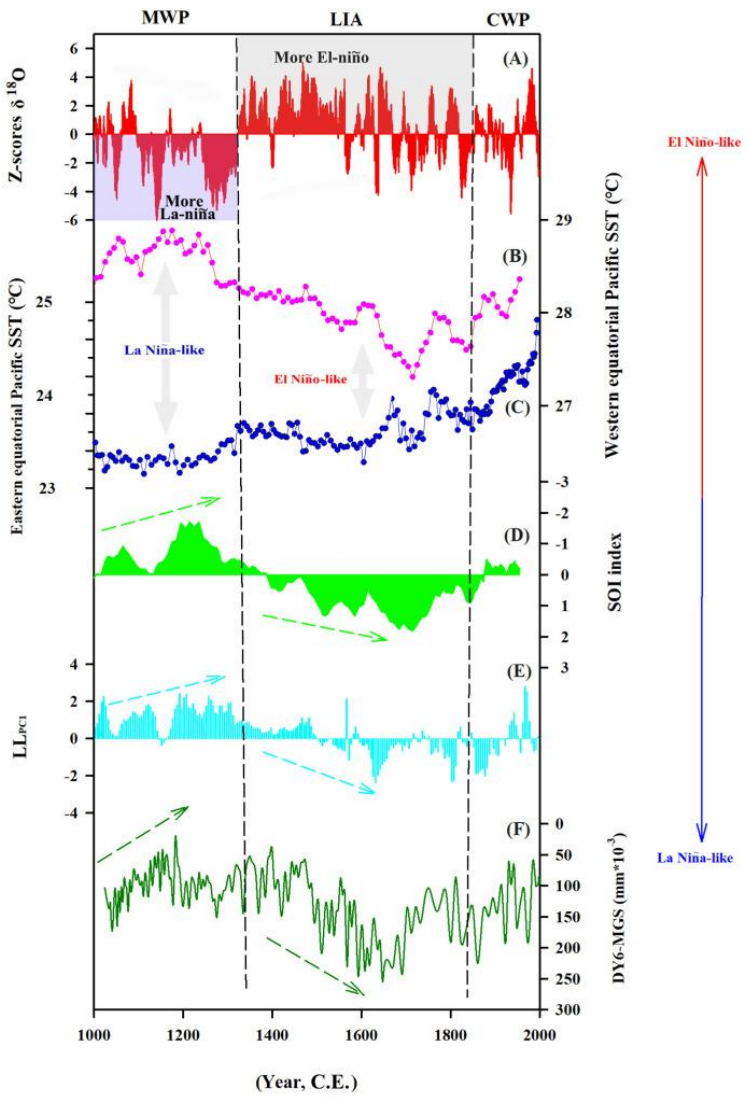

Figure 2. Comparison of reconstructed ENSO variations and tropical Pacific hydrological records. (A) Stalagmite $\delta^{18}O$ Z-scores in the AAM region (this study). (B) Reconstructed SST of the western equatorial Pacific (Indo-Pacific Warm Pool). (C) SST reconstruction of the eastern equatorial Pacific. (D) Reconstructed SOI based on precipitation in the Pacific Ocean. (E) Flores LLPC1 stalagmite record (original data have been processed by an un-rotated principal components analysis, referred to in Liang Luar on the east Indonesian island. (F) Lake sediment mean grain size of Dongdao Island, South China Sea. Noted that, in the MWP and LIA periods, different reconstructed ENSO variations exhibited an opposite trend. The dashed arrows indicate the changing trend of paleoclimate records. The zonal gradient of tropical Pacific SST was decreased in LIA compared with that in the MWP period (B and C).

4. 越南中南部大陆边缘演化及其与南海打开的关系

翻译人：刘伟 inewway@163.com

Nguyen H H, Carter A, Van Hoang L, et al. ***Evolution of the continental margin of south to central Vietnam and its relationship to opening of the South China Sea (East Vietnam Sea)*** *[J]. Tectonics, 2022: e2021TC006971.*

https://doi.org/10.1029/2021TC006971.

摘要：越南南部到中部的大陆边缘以其高海拔高原为特征，其中许多高原被晚新生代的玄武岩流所覆盖。它形成了中国南海广阔大陆裂谷的最西端边缘，隆起被认为是裂谷作用或者是较年轻的板内玄武岩岩浆作用的结果。为了研究这一大陆边缘演化历史，对越南南部到中部边缘的密集样品进行了热年代学研究。结果显示了一个明显的 37 -30 Ma 之间区域快速冷却阶段，之后冷却速率保持低。这一快速冷却阶段时间恰好与南海周缘大陆破裂之前的快速伸展时期一致。我们利用热模拟来检测可能影响冷却的不同地质模型，包括一个明显的剥露增加模型（裂陷作用模型），剥露量减少但随之而来的地温梯度的瞬态下降模型（岩浆作用模型），以及与裂谷作用相一致的是底板作用模型。中生代弧岩浆作用后的热松弛现象被排除（岩浆作用模型），因为地温在岩浆侵位后 20 M.y.内回到了背景速率，远早于快速冷却的开始。模拟支持快速冷却归因于裂陷早期的加速剥露侵蚀。另外也可能会有一些来自下层底板作用和/或热地幔上升流的影响。没有证据支持板块内岩浆作用、季风驱动侵蚀增强或海底扩张动力学相关的区域隆起。

ABSTRACT: The continental margin of south to central Vietnam is notable for its high elevation plateaus many of which are covered by late Cenozoic basalt flows. It forms the westernmost margin of a wide continental rift of the South China Sea (East Vietnam Sea), and uplift has been considered a result of either rifting or younger intraplate basalt magmatism. To investigate margin development apatite thermochronometry was applied to a dense array of samples collected from across and along the margin of south to central Vietnam. Results, including thermal history models, identified a distinct regional episode of fast cooling between c. 37 and 30 Ma after which cooling rates remained low. The fast cooling coincides with a period of fast extension across the South China Sea (East Sea)

region that preceded continental break-up recorded by Oligocene grabens onshore. A thermal model is used test different processes that might influence the inferred cooling including a distinct pulse of exhumation; a decrease in exhumation followed by an associated transient decrease in geothermal gradients and, underplating coincident with rifting. Thermal relaxation following Mesozoic arc magmatism is ruled out as geotherms returned to background rates within 20 Myrs of emplacement, well before the onset of fast cooling. Models support fast cooling attributed to accelerated erosion during early stages of rifting. Some additional heating from either underplating and/or hot mantle upwellings is also possible. No evidence was found to support regional uplift associated with the intraplate magmatism, enhanced monsoon-driven erosion, or seafloor spreading dynamics.

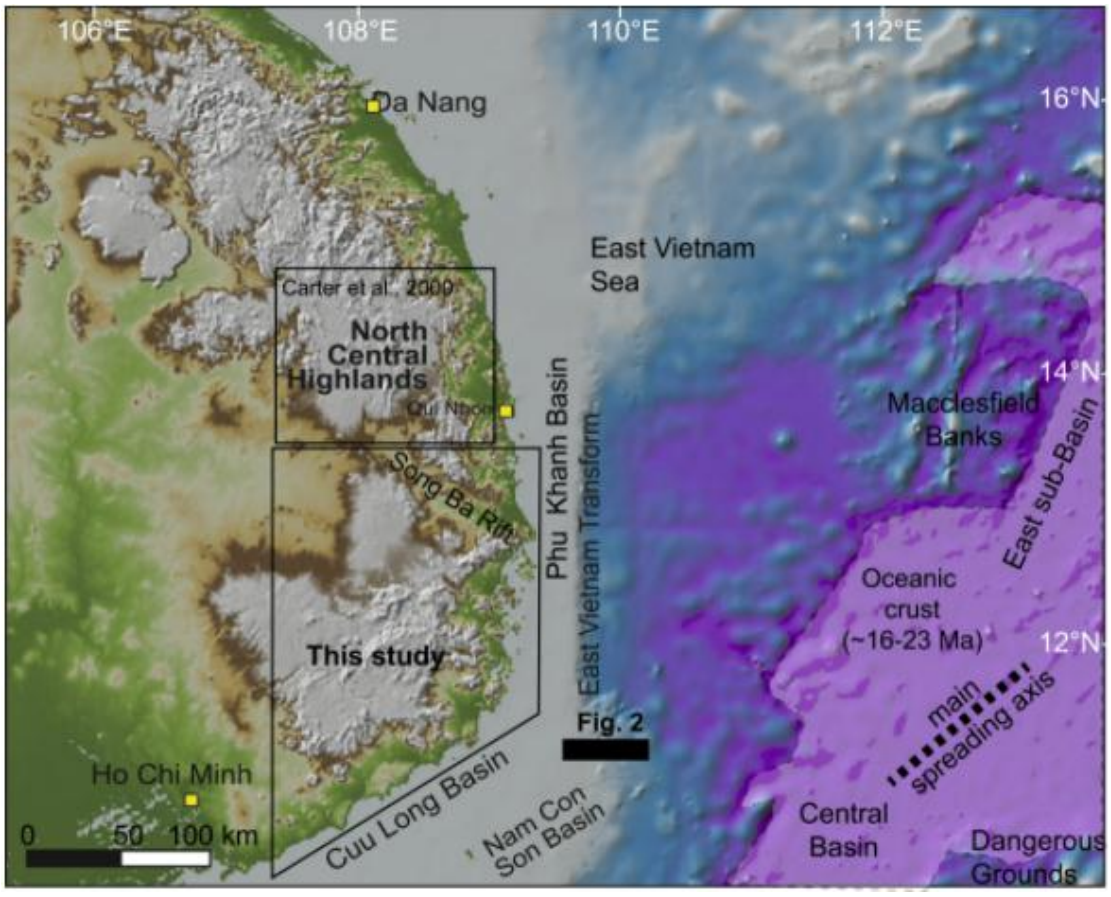

Figure 1. Location of the study area that compliments an earlier study of the Kontum region (Carter et al., 2000).

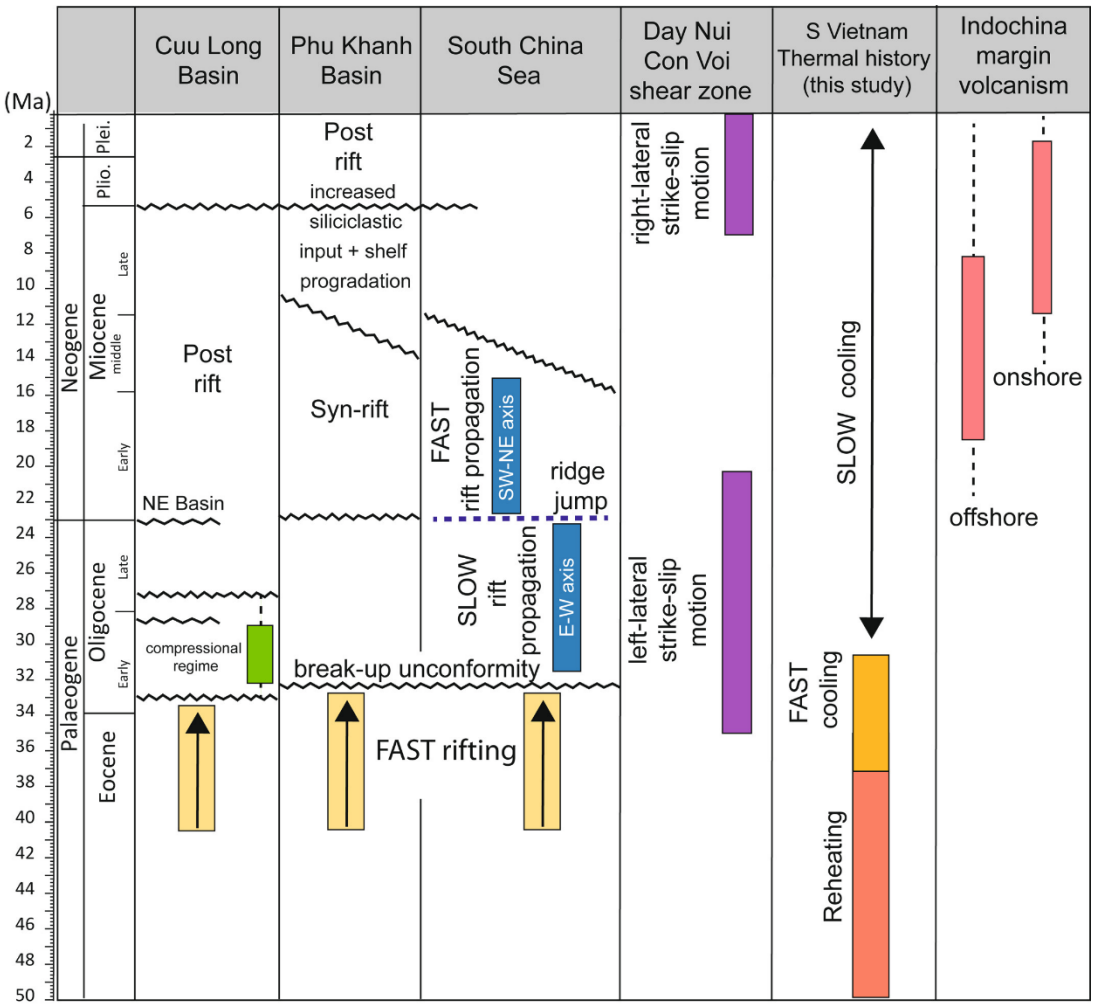

Figure 2. Principal features of the marine basins adjacent to the study area (Fyhn, Boldreel, & Nielsen, 2009; Morley et al., 2019; Schmidt et al., 2019; Vu et al., 2021) compared to the spreading history of the South China Sea (Larsen, 2018; Le Pourhiet et al., 2018), exhumation data, and volcanism across the Indochina margin (Hoang et al., 2013).

5. 2020 年江淮流域极端梅雨的异常特征及其大尺度环流的成因

翻译人：杨会会 11849590@mail.sustech.edu.cn

Niu R Y, Zhai P M, Tan G R, ***Anomalous Features of Extreme Meiyu in 2020 over the Yangtze-Huai River Basin and Attribution to Large-Scale Circulations [J].*** *Journal of Meteorological Research, 2021, 35(5):799-814*

https://doi.org/10.1007/s13351-021-1018-x

摘要：本研究基于梅雨监测信息和降水、全球大气再分析和海表温度（SST）的日资料，从大尺度环流角度调查分析了 2020 年江淮流域（YHRB）梅雨异常特征及其成因。主要结果如下：（1）2020 年 YHRB 梅雨季表现出自 20 世纪 80 年代以来最为显著的异常特征。2020 年的梅雨季节出现时间第 4 早、撤退时间第 3 晚、持续时间最长、梅雨雨量最大、平均降雨强度最强、有暴雨的台站/天最多。（2）2020 年梅雨季节持续时间极长，其原因在于这一特定年份的梅雨出现得早而退得晚。梅雨早发的原因是受 5 月底至 6 月初弱冷空气活动的影响，随着东亚夏季风迁移的西北太平洋副热带高压（NWPSH 和南亚高压（SAH）等主要影响系统早于平常的北移。然而，梅雨极晚的撤退是由于与大尺度环流系统有关的较晚的第二次北移，并伴有较强的冷空气活动，以及 7 月西北太平洋 ITCZ 极弱且偏南。（3）这个比正常梅雨更极端的梅雨季降雨具有持续时间长、降雨强度大等特点。后者可能是由于江淮流域上空水汽辐合和垂直上升运动的极端异常，这是 NWPSH 向西延伸扩张、SAH 向东延伸扩张、低层南风伴随的强水汽输送的综合作用的结果。热带印度洋地区极其温暖的海表温度似乎是诱发上述大尺度异常环流的关键因素。研究结果有助于提高对中国极端梅雨形成机制的认识，并可帮助预报人员从数值模型结果中提取有用的大尺度环流特征，以改进中等详尽的可操作性天气预报。

ABSTRACT: Extremely anomalous features of Meiyu in 2020 over the Yangtze–Huai River basin (YHRB) and associated causes in perspective of the large-scale circulation are investigated in this study, based on the Meiyu operational monitoring information and daily data of precipitation, global atmospheric reanalysis, and sea surface temperature (SST). The main results are as follows. (1) The

2020 YHRB Meiyu exhibits extremely anomalous characteristics, which are the most prominent since the 1980s. The 2020 Meiyu season features the fourth earliest onset, the third latest retreat, the longest duration, the maximum Meiyu rainfall, the strongest mean rainfall intensity, and the maximum number of stations/days with rainstorm. (2) The extremely long duration of the 2020 Meiyu season lies in the farily early onset and late retreat of Meiyu in this particular year. The early onset of Meiyu is due to the earlier-than-normal first northward shift and migration of the key influential systems including the northwestern Pacific subtropical high (NWPSH) and the South Asian high (SAH) along with the East Asian summer monsoon, induced by weak cold air activities from late May to early mid-June. However, the extremely late retreat of Meiyu is because of later-than-normal second northward shift of the associated large-scale circulation systems accompanied with strong cold air activities, and extremely weak and southward located ITCZ over Northwest Pacific in July. (3) The extremely more than normal Meiyu rainfall is represented by its long duration and strong rainfall intensity. The latter is likely attributed to extreme anomalies of water vapor convergence and vertical ascending motion over the YHRB, resulting from the compound effects of the westward extended and enlarged NWPSH, the eastward extended and expanded SAH, and the strong water vapor transport associated with the low-level southerly wind. The extremely warm SST in the tropical Indian Ocean seems to be the key factor to induce the above-mentioned anomalous large-scale circulations. The results from this study serve to improve understanding of formation mechanisms of the extreme Meiyu in China and may help forecasters to extract useful large-scale circulation features from numerical model products to improve medium-extended-range operational forecasts.

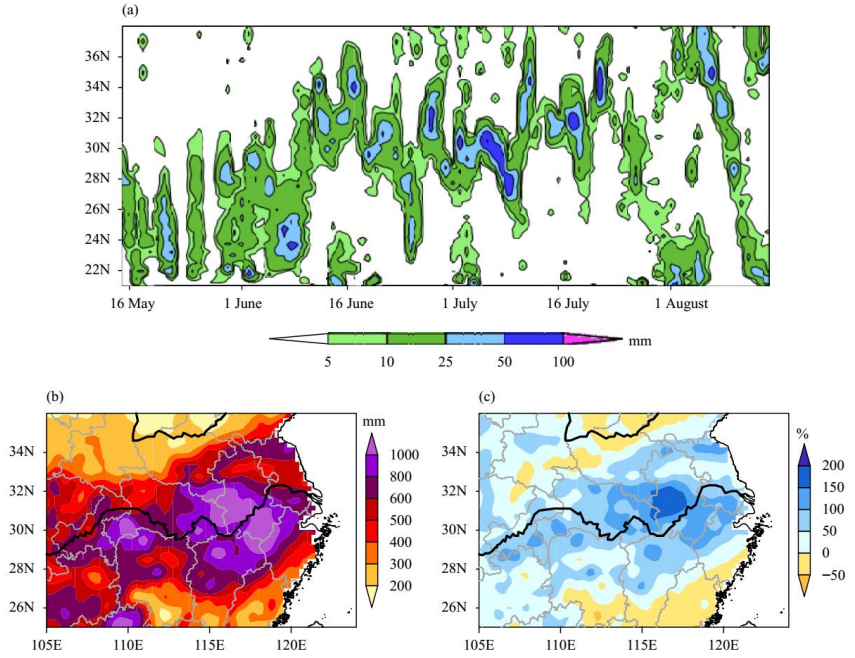

Figure 1. (a) Time–latitude evolution of daily precipitation averaged over 110°–123°E from May to August, and distributions of (b) accumulated precipitation and (c) its percentage anomalies during the Meiyu season over the YHRB in 2020.

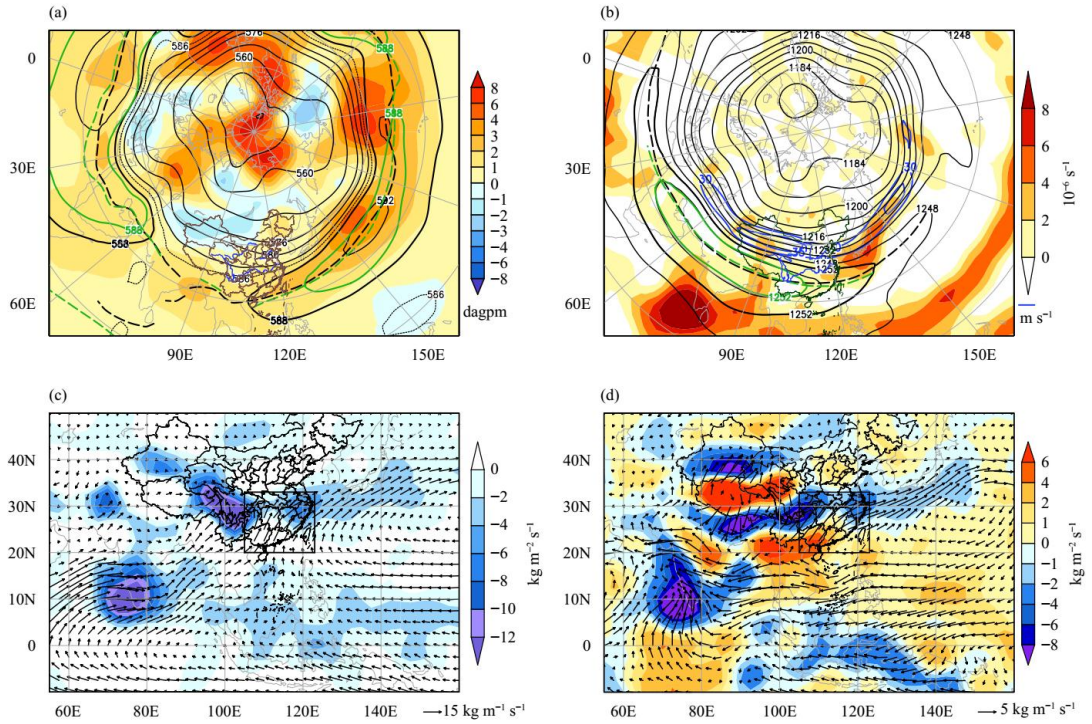

Figure 2. Mean large-scale circulations for the Meiyu season of 2020: (a) geopotential height (black solid lines) and its anomalies (shading) at 500 hPa, (b) geopotential height (black solid lines), zonal wind greater than 30 m s^{-1} (blue lines), and divergence (shading) at 200 hPa, (c) water vapor flux (vector) and its divergence (shading) at 850 hPa, (d) anomalies of water vapor flux (vector) and its divergence (shading) at 850 hPa. In (a) and (b), the bold black solid lines show the range of the subtropical highs at 500 hPa and the SAH at 200 hPa denoted by the 588- and 1252- dagpm isolines respectively; the black dashed lines show the ridge line of the highs; and the green lines show the climatic range and ridge line of the highs. The rectangle in (c) and (d) denotes the region 20 °–33 °N, 105 °–123 °E.

6. 地壳氧化状态的证据—来自锰矿物的演化

翻译人：张亚南 zhangyn3@mail.sustech.edu.cn

Hummer D R, Golden J J, Hystad G, et al. ***Evidence for the oxidation of Earth's crust from the evolution of manganese minerals*** *[J]. Nature Communications, 2022,13, 960.*

https://doi.org/10.1038/s41467-022-28589-x

摘要：通过锰矿物的赋存状态和价态的分析，揭示了地壳随时间推移发生的氧化作用。地壳氧化还原状态的变化对地球的演化至关重要，但对空间上地壳的平均氧化还原状态评估的方法却很少。锰（Mn）作为一种氧化还原敏感元素，其多变的氧化状态及在地壳中丰富的含量，使其成为一种有效的地壳氧化状态示踪剂。文中，作者发现地壳锰元素的平均氧化状态增多，对应了过去 10 亿年里的大气氧化事件，但滞后了 66±1 Ma。作者将这一滞后时间解释为地壳浅层与大气氧逸度平衡所必须的时间。该研究利用大量的矿物学数据库来评估地球演化历史中的地球化学条件，作者认为这一矿物数据集和其他矿物数据集构成了一类重要的指标来约束地球各储层的氧化还原状态演化。

ABSTRACT: Analysis of manganese mineral occurrences and valence states demonstrate oxidation of Earth's crust through time. Changes in crustal redox state are critical to Earth's evolution, but few methods exist for evaluating spatially averaged crustal redox state through time. Manganese (Mn) is a redox-sensitive metal whose variable oxidation states and abundance in crustal minerals make it a useful tracer of crustal oxidation. We find that the average oxidation state of crustal Mn occurrences has risen in the last 1 billion years in response to atmospheric oxygenation following a 66 ± 1 million-year time lag. We interpret this lag as the average time necessary to equilibrate the shallow crust to atmospheric oxygen fugacity. This study employs large mineralogical databases to evaluate geochemical conditions through Earth's history, and we propose that this and other mineral data sets form an important class of proxies that constrain the evolving redox state of various Earth reservoirs.

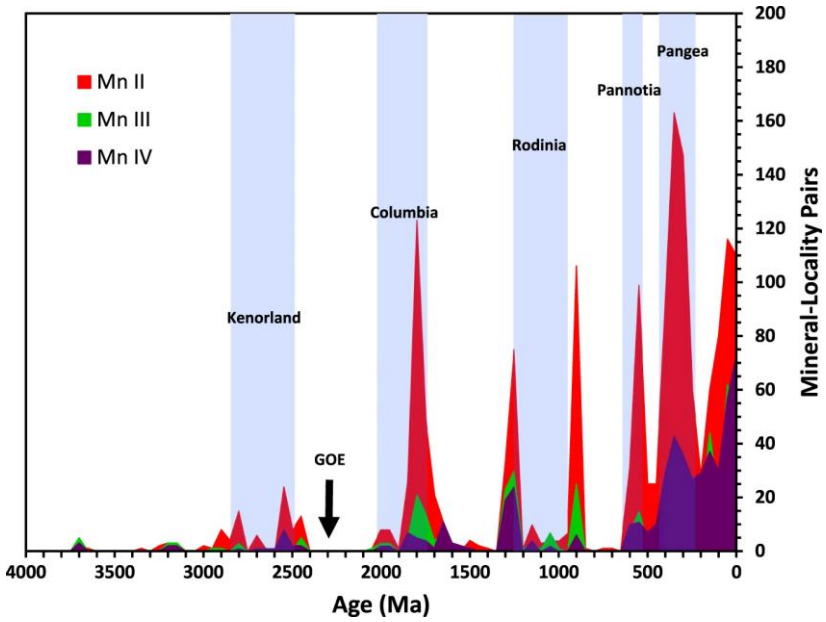

Figure 1. Mn mineral occurrence histogram. A histogram showing the number of occurrences of mineral-locality pairs as a function of geologic time for all dated Mn-bearing mineral species, with data parsed into 50 million-year bins. Colors indicate oxidation state of Mn; Red = Mn(II), Green = Mn(III), Purple = Mn(IV). Blue bands represent intervals in which Earth's major landmasses are thought to have consolidated into a supercontinent.

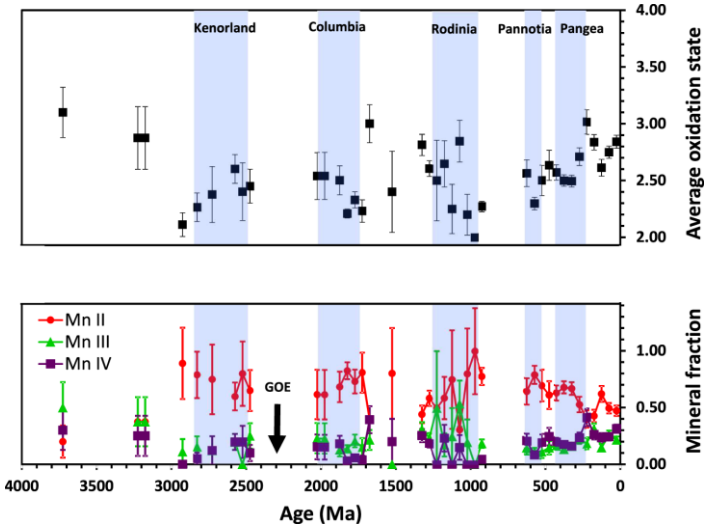

Figure 2. Individual and average Mn oxidation states as a function of geologic time. Graph of fraction of Mn mineral occurrences (lower) and average Mn oxidation state (upper) as a function of geologic time, with data parsed into 50 million-year bins. Colored symbols indicate oxidation state of Mn; Red circles = Mn(II), Green triangles = Mn(III), Purple squares = Mn(IV). Blue bands represent intervals in which Earth's major landmasses are thought to have consolidated into a supercontinent. Uncertainties for oxidation state fractions are standard deviations calculated as the square root of the number of counts for

an oxidation state divided by the total counts for all oxidation states in a given time bin, using an approximation from the negative binomial distribution as described in "Methods".

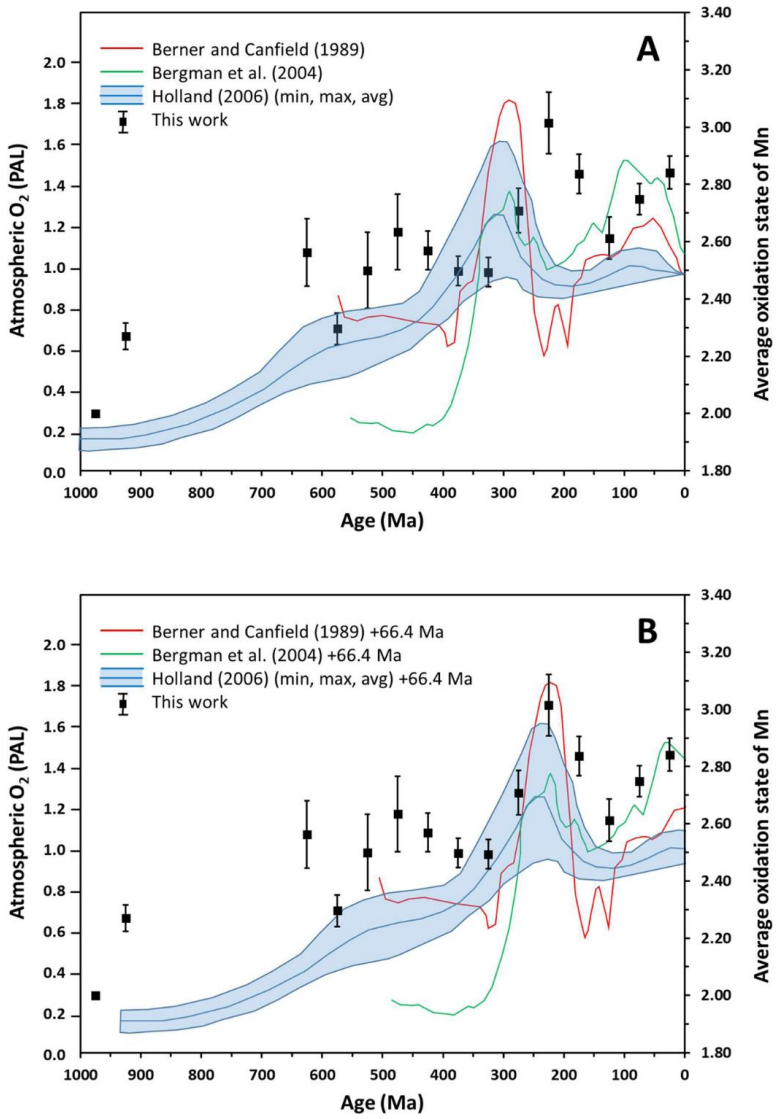

Figure 3. Comparison of average Mn oxidation state with atmospheric O_2 reconstructions. **A** Graph of the average oxidation state of Mn according to Mn mineral occurrences (black squares, right vertical axis) over the most recent 1 billion years, overlain with reconstructions of atmospheric oxygen (left vertical axis) by Berner and Canfield (red line), Bergman et al. (green line), and the O_2 concentration range including minimum, average, and maximum by Holland (blue lines). Uncertainties regarding the Mn oxidation state data points are standard deviations calculated (assuming a Poisson distribution of mineral-locality counts) as the square root of the sums of the variances of counts for the individual oxidation states according to propagation of errors. **B** Graph of the average oxidation state of Mn according to Mn mineral occurrences (black squares) over the most recent 1 billion years, overlain with reconstructions of atmospheric oxygen by Berner and Canfield (red line), Bergman et al. (green line), and the O_2

concentration range including minimum, average, and maximum by Holland (blue lines), but with oxygen reconstructions shifted forward in time by 66.4 Myr. Note that when this time lag is accounted for, the average oxidation state of Mn in the geologic record displays a trend of minima and maxima that coincide closely with atmospheric oxygen concentrations.

7. 海岸黄土沉积约束渤海近 200 ka 的海平面变化

翻译人：李海 12031330@mail.sustech.edu.cn

Yi S, Zeng L, Xu Z, et al. ***Sea-level changes in the Bohai Sea, northern China, constrained by coastal loess accumulation over the past 200 ka*** *[J]. Quaternary Science Reviews, 2022, 277: 107368.*

https://doi.org/10.1016/j.quascirev.2021.107368

摘要:黄土广泛分布在半干旱地区，海岸带地区也有分布。沿海黄土的堆积为气候和海平面变化提供了宝贵的记录。本研究，作者报告了渤海沿岸和庙岛群岛的两个黄土沉积序列的沉积学和高分辨率光释光测年记录。石英光释光和钾长石红外 IRSL ($pIRIR_{290}$)信号在~100 ka 内表现一致，钾长石 $pIRIR_{290}$ 可以提供~200 ka 的年龄控制点。基于这个年龄模型，作者认为沿海的黄土堆积是偶发的，堆积速率变化很大。通过与全球及区域海平面记录对比，高沉积速率时期与全球低海平面阶段相吻合，沉积速率接近零或极低的黄土沉积时期主要对应于全球高海平面阶段，表明全球海平面变化对研究区沿海黄土堆积起主导作用。研究结果表明，区域海退主要发生在 MIS 6 和 MIS 5b 至 MIS 2 期间，区域性极低的海平面发生在~150 ka，70-60 ka 和 37-24 ka 期间。MIS 5e–5c 和 MIS 1 表现为高海平面。这一研究表明，具有良好年代学资料的沿海黄土沉积物可用于约束区域海平面变化的时间。

ABSTRACT: Loess sequences are widely distributed in semi-arid regions around the world, and are sometimes also located in coastal zones. The accumulations of coastal loess provide a valuable record of both climate and sea-level changes. Here we report sedimentological and high sampling resolution luminescence dating evidence for such changes from two loess sequences from the Shandong Peninsula and Miaodao Archipelago near the coast of Bohai Sea in northern China. Both the quartz optically stimulated luminescence (OSL) and K-feldspar post-infrared IRSL ($pIRIR_{290}$) signals show consistent and satisfactory luminescence characteristics up to ~100 ka, while the K-feldspar $pIRIR_{290}$ ages provide age control up to ~200 ka and are in stratigraphic order. With this fully independent age model, our results reveal that coastal loess accumulation is episodic with a high variability in apparent accumulation rates. After comparing with global and regional sea-level

records, we find that the intervals with high accumulation rates coincide with global low sea-level stages, and that the loess sedimentary hiatuses indicated by nearly zero or very low accumulation rates at one site mainly correspond to global high sea-level stages, indicating the dominant role of global sea-level changes on coastal loess accumulation in the study area. We therefore conclude that regional marine regression mainly occurred during MIS 6, and MIS 5b to MIS 2, with extremely low regional sea levels possibly around 150 ka, 70–60 ka and 37–24 ka, while high sea-levels occurred during MIS 5e–5c and MIS 1. This study implies that coastal loess deposits with a good chronology could be used to constrain the timing of regional sea level change.

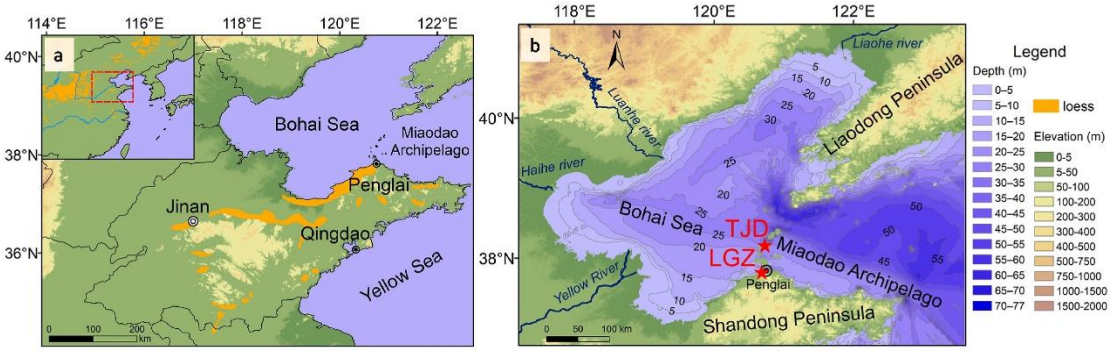

Figure 1. (a) Loess distribution in Shandong Province, North China. (b) Elevation map showing the location of the LGZ and TJD loess sections.

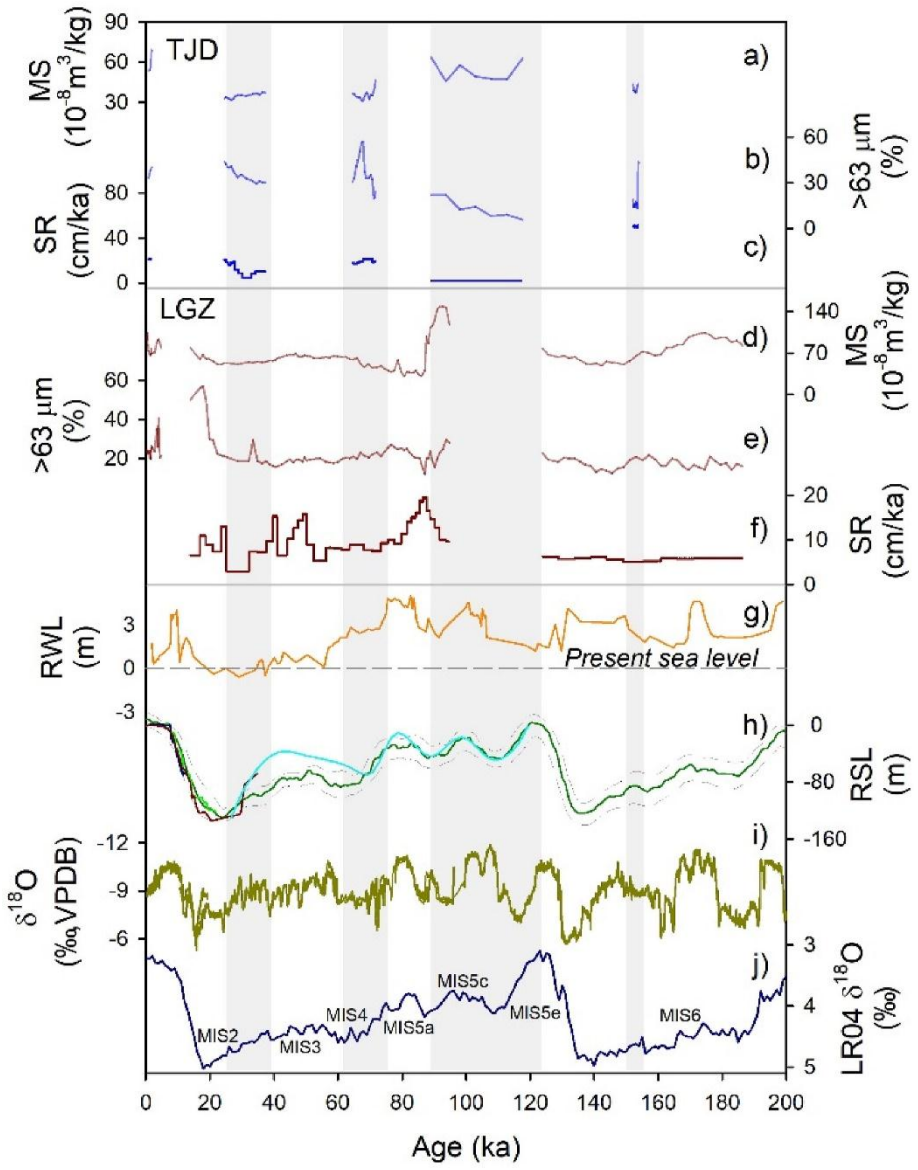

Figure 2. Comparison of loess records with other independent reconstructions of sea-level changes over the last 200 ka. (a), (b), (c), (d), (e) and (f) Magnetic susceptibility (MS), grain size (>63 μm), and loess sedimentation rate (SR) of TJD and LGZ, respectively. (g) Reconstructed relative sea level in the south Bohai Sea since the late Pleistocene (RWL: reference water level, Yi et al., 2015). (h) Global sea-level changes during different periods (RSL: relative sea-level, Lambeck et al., 2014; Xue, 2014; Spratt and Lisiecki, 2016; Pico et al., 2016). (i) Stalagmite δ18O record from Sanbao-Hulu caves (Wang et al., 2008; Cheng et al., 2009). (j) Benthic foraminiferal δ18O record from marine stack LR04 (Lisiecki and Raymo, 2005).

8. Saint Helena 低古强度和 Ar/Ar 定年提供南大西洋反复出现弱磁场的证据

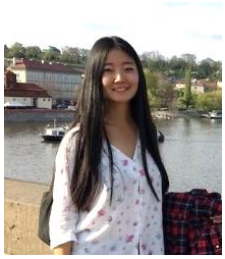

翻译人：张琪 zhangq7@sustech.edu.cn

Engbers Y A, Grappone J M, Mark D F, et al., ***Low paleointensities and Ar/Ar ages from Saint Helena provide evidence for recurring magnetic field weaknesses in the South Atlantic*** *[J]. Journal of Geophysical Research: Solid Earth, 2022, e2021JB023358.*

https://doi.org/10.1029/2021JB023358

摘要：南大西洋异常(SAA)是现今地磁异常中最显著的弱磁区域。尽管存在这样的异常现象，长期以来一直存在一个假设，如果在足够长的时间内(10^4 - 10^6 年)，地球磁场近似于地心轴偶极子(GAD)。非地心轴向偶极子特征在时间平均场中的重要性是一个重要且尚未解决的问题。在历史和古地磁场模型中，SAA 并不总是可见的；然而，在数百万年的时间尺度上，南大西洋地区存在一个不稳定的磁场。这项研究首次对 Saint Helena 进行了古强度研究。Saint Helena 是南大西洋的一个火山岛，主要由 8 - 10 Ma 之间喷发的熔岩形成。虽然古强度测量的成功率较低，但作者仍然成功的从 5 个独立的熔岩体中恢复出古地磁场数据，结果表明，低场强为 10.5±3.0 μT，对应的虚拟轴向偶极矩(VADM)为 $2.4\pm0.7\times10^{22}$ Am^2。这些较低的古强度估计表明，南大西洋的磁场不仅在方向上不稳定，而且比预期的要弱得多。作者认为这进一步证明了 SAA 不是一个单一的现象，而是该地区一系列重复出现的弱场的最新一个，可能是由核幔边界上的反向通量块引起的。

ABSTRACT: The South Atlantic Anomaly (SAA) is an area of geomagnetic weakness that represents the most significant anomaly in the present-day field. Notwithstanding anomalies such as these, a long-lived hypothesis is that, if averaged over sufficient time (10^4-10^6 years), the Earth's magnetic field approximates a geocentric axial dipole (GAD). The question of how significant the non-GAD features are in the time-averaged field is an important and unresolved one. The SAA has not always been visible in the historic and paleo- field models; yet an unstable field was reported in the South Atlantic region on a multi-million-year timescale. This study presents the first paleointensity study from Saint Helena, a volcanic island in the South Atlantic consisting primarily

of lavas emplaced between 8 and 10 Ma. While paleointensity success rates were low, we were able to recover results from 5 independent lavas that together suggest a low field intensity of 10.5 ± 3.0 μT corresponding to a virtual axial dipole moment (VADM) of 2.4 ± 0.7 × 10^{22} Am^2. These low paleointensity estimates suggest a field in the South Atlantic that was not only unstable in directions, but also substantially weaker than expected. We consider this to constitute further evidence that the SAA is not a single occurrence but rather, the latest in a series of recurring weaknesses in the field in this region, probably caused by Reversed Flux Patches on the Core Mantle Boundary.

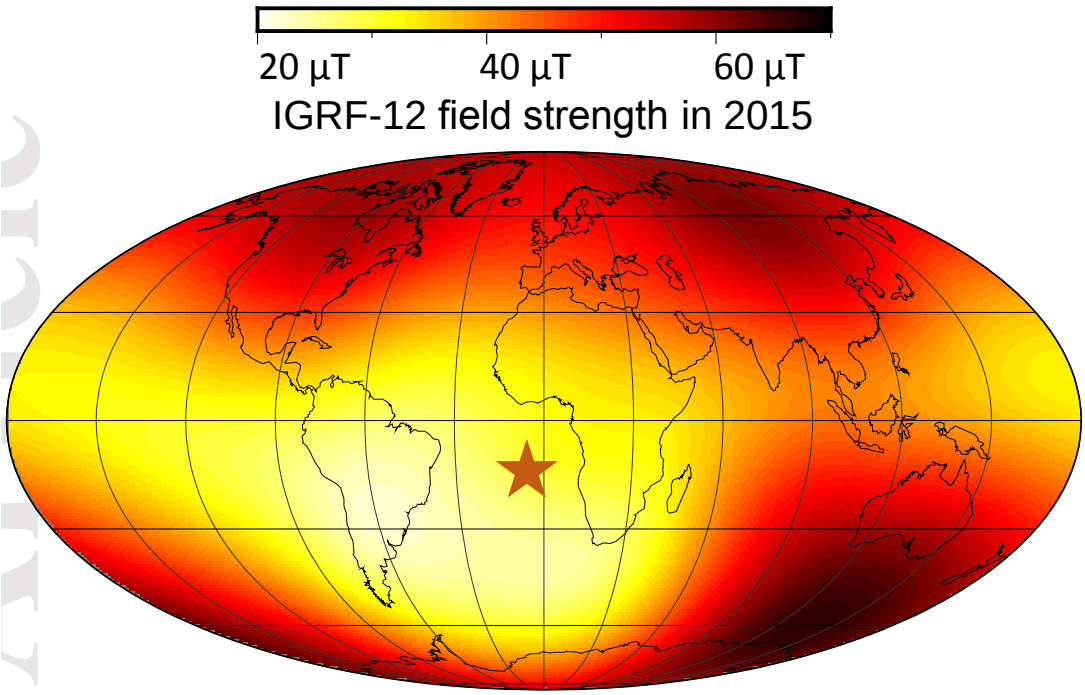

Figure 1. Magnetic field strength from IGRF-12 (Thébault et al., 2015). The orange star is Saint Helena.

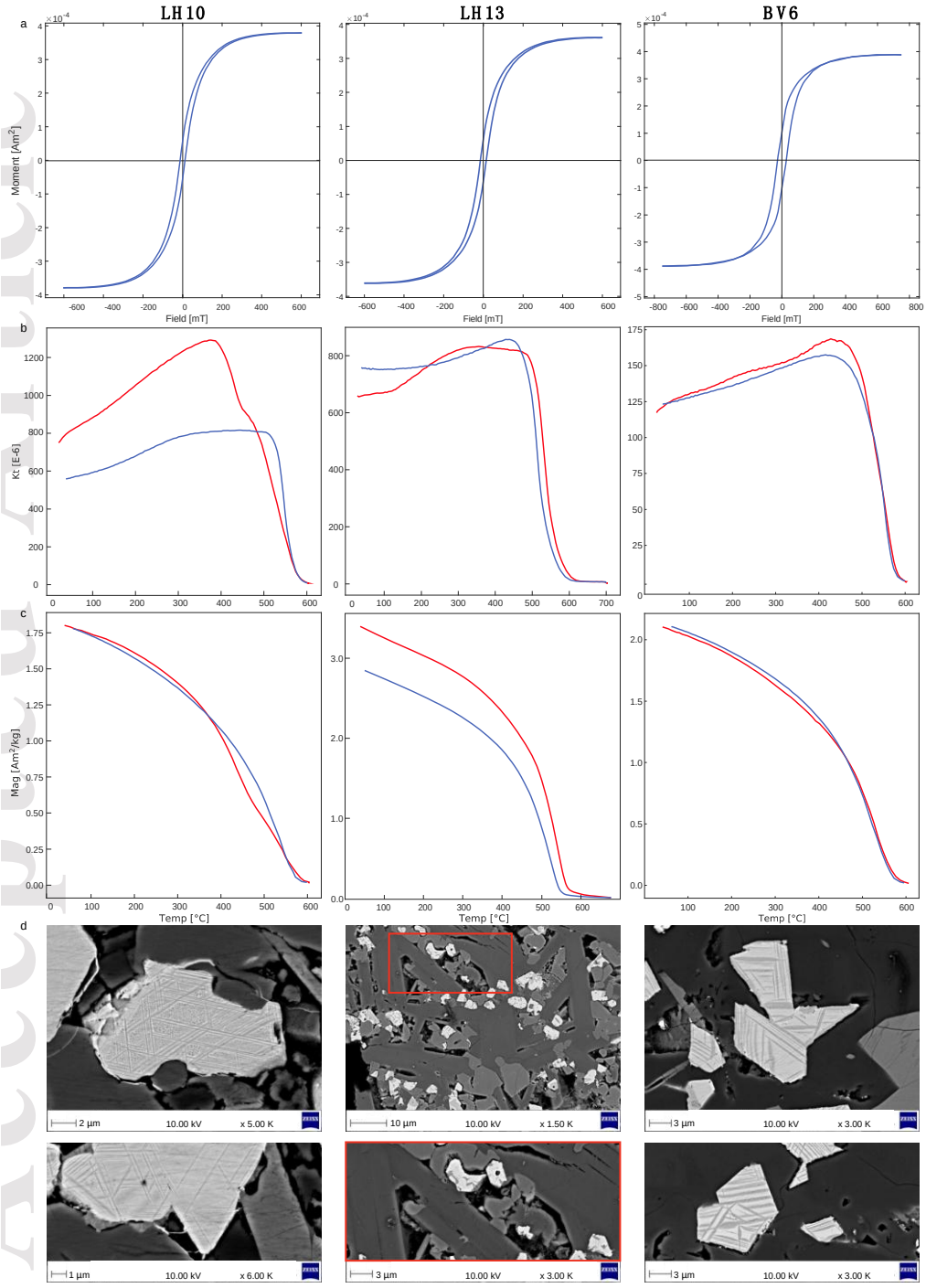

Figure 2. Rock magnetic behaviour for 3 sites that yielded successful paleointensity estimates (LH10, LH13 and BV6). Subplot a. Hysteresis loops that were paramagnetically corrected; Subplot b. High temperature susceptibility curves, red is heating curve and blue is cooling curve); Subplot c. Thermo-magnetic curves (as in b); Subplot d) SEM BSE images showing oxidation lamellae (Ox. Class IV for LH10, III for LH13 and BV6). For LH13 the lowermost BSE image is the zoomed in area represented by the red square in the BSE image above.

9. 斜长石中定向磁铁矿包裹体：对剩磁各向异性的影响

翻译人：张伟杰 12031188@mail.sustech.edu.cn

Ageeva O, Habler G, Gilder S A, et al. ***Oriented Magnetite Inclusions in Plagioclase: Implications for the Anisotropy of Magnetic Remanence*** *[J]. Geochemistry, Geophysics, Geosystems, 2021: e2021GC010272.*

https://doi.org/10.1029/2021GC010272

摘要：造岩硅酸盐矿物中微米到亚微米的铁磁性包裹体可能会携带特别稳定的剩磁。当包裹体在岩石中具有结晶或形状排列优选方向时，所记录的古地磁方向和强度可能会因磁各向异性而有所偏差。为了更好地理解这一效应，我们对位于 11-17 ℃N 的中大西洋洋脊的大洋辉长岩中的斜长石颗粒展开了研究。斜长石颗粒中含有大量沿斜长石晶格特定方向排列的针状和条状磁铁矿包裹体。电子背向散射衍射和剩磁各向异性测试被用来关联包含多个双晶类型（曼尼巴律、卡斯巴律、钠长石律、肖纳长石律）的宿主斜长石中磁铁矿包裹体的取向分布与其整体磁各向异性之间的关系。未被改造的斜长石的剩磁各向异性椭球为平行于斜长石（010）平面的饼状。结果表明，在热液叠改造程中，磁铁矿包裹体的重结晶作用改变了不同取向类别的包裹体的相对丰度。结果展示了剩磁各向异性椭球的最大轴与斜长石[001]方向平行，这反过来控制了获得剩磁的方向。我们的研究结果可用于古强度和古方向的确定以及磁组构的解释。

ABSTRACT: Micron to sub-micron sized ferromagnetic inclusions in rock forming silicate minerals may give rise to particularly stable remanent magnetizations. When a population of inclusions have a preferred crystallographic or shape orientation in a rock, the recorded paleomagnetic direction and intensity may be biased by magnetic anisotropy. To better understand this effect, we investigated plagioclase grains from oceanic gabbro dredged from the Mid-Atlantic Ridge at 11-17 ℃N. The plagioclase grains contain abundant needle and lath shaped magnetite inclusions aligned along specific directions of the plagioclase lattice. Electron back scatter diffraction and anisotropy of magnetic remanence measurements are used to correlate the orientation distribution of the magnetite inclusions in the host plagioclase that contains multiple twin types (Manebach, Carlsbad, Albite and Pericline) with the bulk magnetic anisotropy of the inclusion-host

assembly. In non-modified plagioclase, the anisotropy ellipsoid of magnetic remanence has oblate shapes that parallels the plagioclase (010) plane. It is suggested that recrystallization of magnetite inclusions during hydrothermal overprint shifts the relative abundance of the inclusions pertaining to the different orientation classes. We show that the maximum axis of the anisotropy ellipsoid of magnetic remanence parallels the plagioclase [001] direction, which in turn controls the recorded remanent magnetization direction. Our results are relevant for paleointensity and paleodirection determinations and for the interpretation of magnetic fabrics.

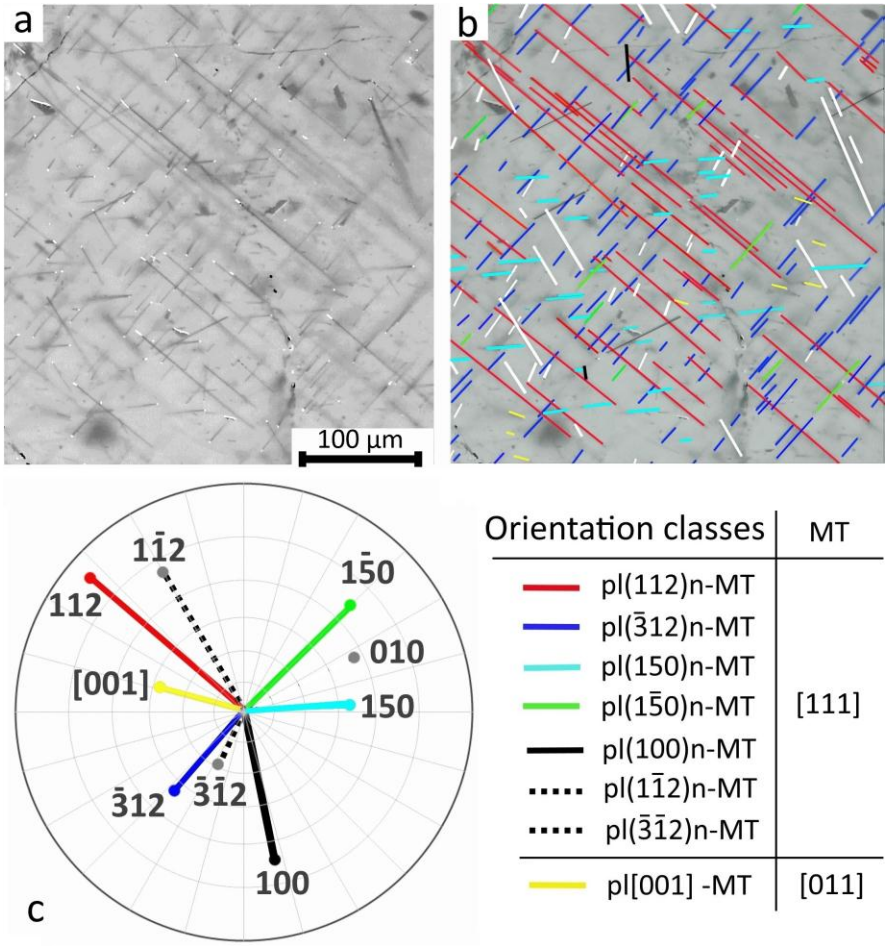

Figure 1. (a) Optical image under combined reflected and transmitted light showing magnetite inclusions in an untwinned domain of plagioclase in sample L30-277-10. (b) Same as in (a) with the magnetite needles color coded according to the orientation class they pertain to. (c) Pole figure of the needle orientations; note that the number of observed pl(112)n-mt needles is less than their true bulk concentration due to their orientation subparallel to the plane of the thin-section, which is only about 30 µm thick, while the field of view is about 300x300 µm^2.

10. 太平洋亚热带高压在南方涛动周期中的作用

翻译人：刘宇星 11811211@mail.sustech.edu.cn

Yafei Wang. ***The role of Pacific subtropical high belts in the ENSO cycle*** *[J]. Tellus A: Dynamic Meteorology and Oceanography, 2019, 71(1): 1-20.*

https://doi.org/10.1080/16000870.2019.1656514

摘要：本文利用常规资料从多个角度对厄尔尼诺和南方涛动(ENSO)的形成进行了统计分析。我们发现如果在计算中假设了年循环对 ENSO 的影响，那么厄尔尼诺和拉尼娜现象都与赤道两侧的太平洋副热带高压(PSH)的初期活动有密切联系。在厄尔尼诺现象成熟之前的几个月里，PSH（尤其是在其东部地区）往往持续减弱。相反，PSH 的持续增强可能被视为拉尼娜现象的前奏。这标志着 PSH 对 ENSO 的预测比来自热带地区的特征早了大约两个月。我们发现，通过影响信风强度的变化，PSH 的加强或减弱可以作为驱动 ENSO 循环的更本源之力。ENSO 循环的锁相也可能是由于该形势下 PSH 在南半球比北半球表现得更强来解释的。此外，由于每年 6 - 8 月南半球 PSH 最接近赤道区域，能够对赤道产生更强的影响，而赤道东太平洋区域的 SST 在 3 - 4 个月后才会受到显著影响，这意味着一般的 ENSO 成熟位相发生在年末左右。我们根据以上结果提出了一个可能的 ENSO 形成机制，并对这个新机制进行了有针对性的讨论，解释了目前 ENSO 模型存在的问题。

ABSTRACT: This article conducted statistical analyses on the formation of El Niño and Southern Oscillation (ENSO) from several angles by using conventional data. We found that both El Niño and La Niña are closely associated with the preliminary activity of the Pacific subtropical high (PSH) belts on both sides of the equator if bringing an assumption of the influence of annual cycle on ENSO cycle into our calculations. The PSH belts, especially in their eastern sides, tended to have been continuous weakening for months before El Niño maturing. Oppositely, the continuous enhancing of the PSH belts might be regarded as a prelude of a La Niña. This signal the PSH belts send to omen ENSO's coming appeared about two months earlier than the one from the elements in

tropical regions. We found that the strengthening or weakening of the PSH belts could act as a more original force for driving the ENSO cycle than the elements in tropics through controlling the variation of trade winds. Since the southern PSH belt appeared more powerful than the northern one in the situation, the phase lock of the ENSO cycle might be explained by this clue. Because the southern PSH belt that approaches the nearest area of the equator every June–August in a calendar year can exert a more powerful impact on equatorial elements, SST in Eastern Equatorial Pacific will be significantly affected 3–4 months later, i.e. the general ENSO mature phase happening around the end of a calendar year. We proposed a plausible mechanism for the ENSO formation based on the results and conducted a targeted discussion on this new mechanism that could explain the problems the current conceptual ENSO models left.

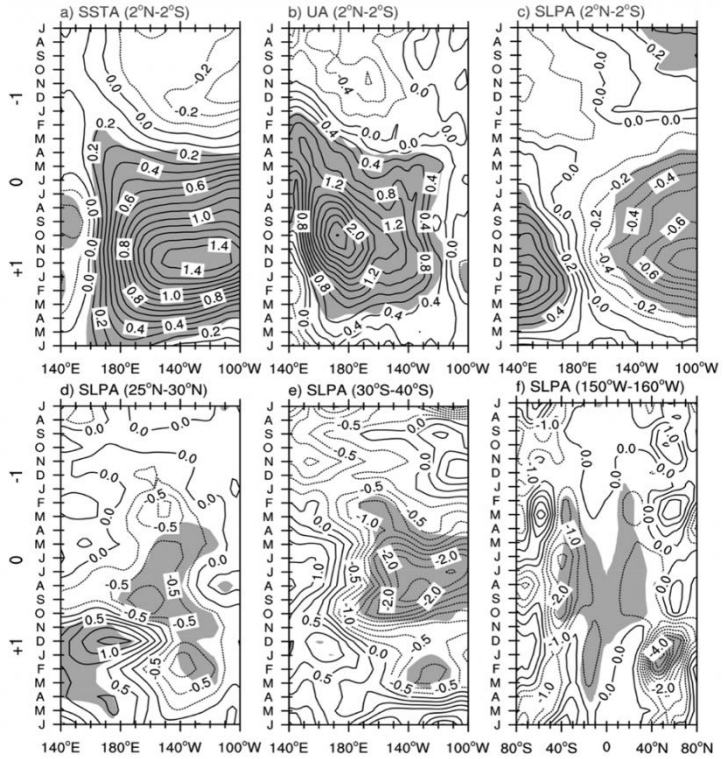

Figure 1. The El Niño composite for SSTa (a, unit: K), surface zonal wind anomalies (b, unit: ms−1), SLPa (c, unit: hPa) averaged between 2 °N and 2 °S; SLPa averaged between 25 °N and 30 °N (d), averaged between 30°S and 40°S (e), averaged between 150°W and 160°W (f) from July of −1 year to June of +1 year. The 0 years for the composite included 1965, 1972, 1976, 1982, 1986, 1987, 1991, 1994, 1997, 2002, 2003, 2006, 2009, 2014, 2015. Shaded areas indicate significance at 95%.

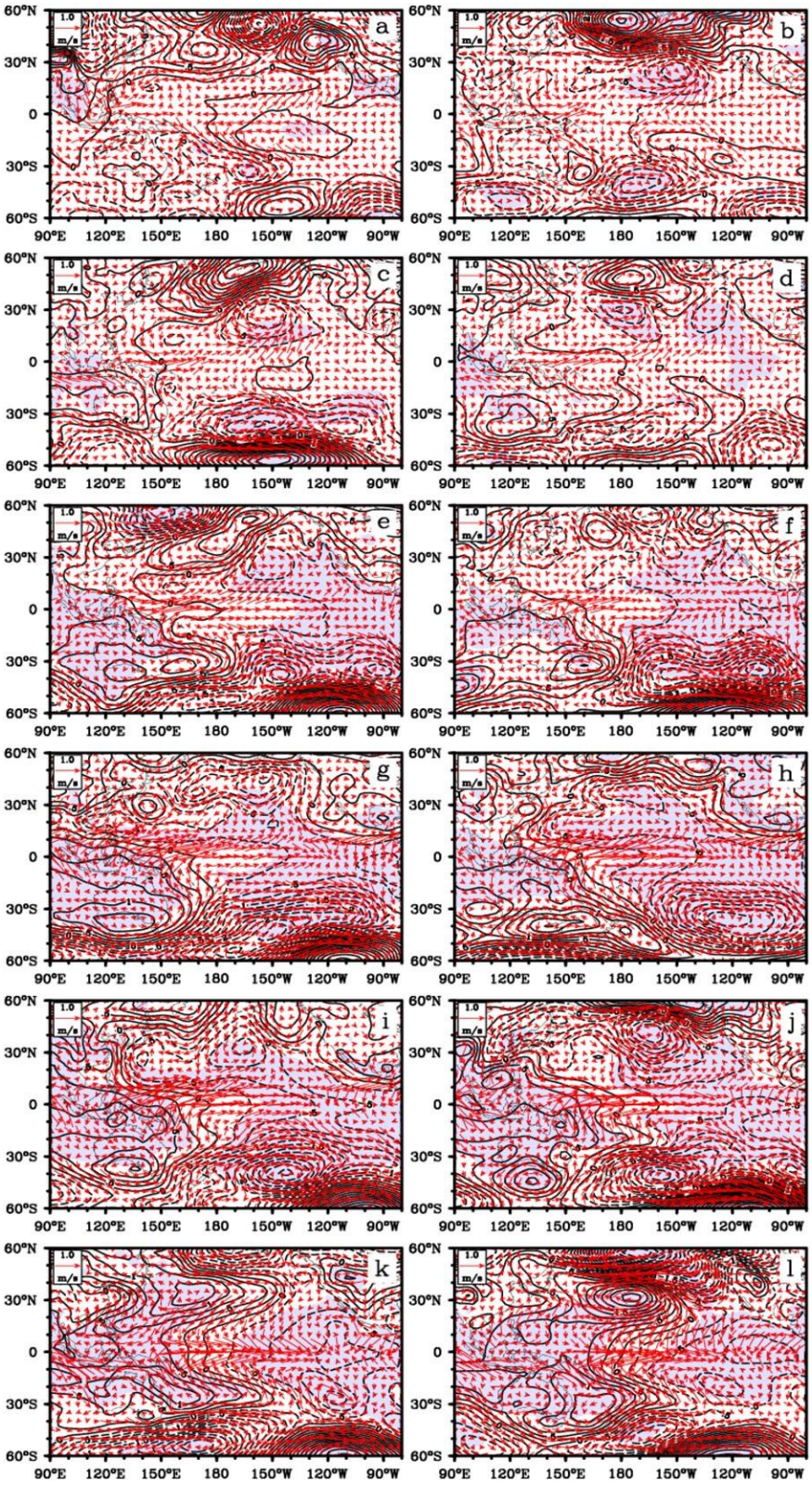

Figure 2. Distributions of SLPa (unit: hPa) and surface wind vector (unit: ms−1) anomalies for El Niño composite from January to December (a–l). Shaded areas indicate the significance at 95%.